

Scalar field theory limits of bosonic string amplitudes

Alberto Frizzo and Lorenzo Magnea*

*Dipartimento di Fisica Teorica, Università di Torino
and I.N.F.N., Sezione di Torino
Via P.Giuria 1, I-10125 Torino, Italy*

Rodolfo Russo

*Institut de Physique, Université de Neuchâtel
Rue A.-L. Breguet 1, CH-2000 Neuchâtel, Switzerland*

Abstract

We describe in detail the techniques needed to compute scattering amplitudes for colored scalars from the infinite tension limit of bosonic string theory, up to two loops. These techniques apply both to cubic and quartic interactions, and to planar as well as non-planar diagrams. The resulting field theories are naturally defined in the space-time dimension in which they are renormalizable. With a careful analysis of string moduli space in the Schottky representation we determine the region of integration for the moduli, which plays a crucial role in the derivation of the correct combinatorial and color factors for all diagrams.

*e-mail: magnea@to.infn.it

1 Introduction

It is well known that all perturbative states in string theory have a squared mass proportional to the string tension T . Thus, in the low energy regime (or zero-slope limit, $\alpha' = 1/(2\pi T) \rightarrow 0$), the heavy string states become infinitely massive and decouple, while the light states survive and their dynamics can be effectively described by an ordinary field theory. It was understood, already in the old days of dual models, that one can define this point-like limit in different ways, so that it is possible to recover different field theories. In the first application of this idea [1], the tree-level amplitudes of a scalar field theory with cubic interactions were derived from the corresponding amplitudes among scalar string states; it was then shown that, if massless spin-1 states are selected, in the low-energy limit one can reproduce the tree diagrams of Yang-Mills theory [2], while, if closed string are considered, one obtains the amplitudes of Einstein's gravity [3, 4].

In more recent years further steps were taken, and string techniques were actually exploited as a *simplifying* tool that can substitute Feynman diagrams for the explicit calculation of scattering amplitudes and other quantities of interest in field theory. For example, effective actions and threshold effects of interest for string unification were computed in [5, 6, 7]; string-inspired techniques were applied to the evaluation of one-loop QCD scattering amplitudes [8, 9, 10, 11, 12] and renormalization constants [13, 14, 15]; graviton scattering amplitudes were computed and their relation to gauge amplitudes explored [16, 17]; progress was made towards the extension of the method to more than one loop [18, 19, 20, 21, 22, 23], to amplitudes with external fermions [24], and to off-shell amplitudes [25]. String techniques also served to stimulate the development of new techniques in field theory, that preserve some of the nice features of the string formalism [26, 27, 28, 29, 30, 31].

At first sight, the use of extended object for constructing particle scattering amplitudes may appear as an unnecessary detour, since one is interested only in the zero-slope limit. However, as is now well understood, this procedure presents many useful features. For instance, string amplitudes are naturally written in a way that takes maximal advantage of gauge invariance, and the color decomposition is automatically performed. At higher order in the perturbative expansion, further advantages become apparent: the loop momentum integrals are already performed, so that helicity methods can be readily employed, and the result for a set of Feynman diagrams of a given topology is presented directly as a Schwinger-parameter integral. Moreover, one does not find the large proliferation of diagrams characteristic of field theories, which makes it extremely difficult to perform high order calculations. In the case of closed strings one gets only one diagram at each order, while in the open string the number of diagrams remains small. Finally, in the case of bosonic strings, the expressions of scattering amplitudes and of the measure of integration on moduli space are known explicitly for an arbitrary perturbative order; in the sewing procedure [32, 33], they can be obtained from tree level diagrams

by identifying pairs of external legs with an appropriate propagator.

On general grounds, a striking difference between field-theoretic and string-derived amplitudes is the degree of correlation in the calculation of different amplitudes in different field theories. In field theory, different amplitudes are largely independent of each other, and thus in each computation one has to start from the same basic ingredients, the Feynman rules; also, results obtained in one theory can rarely be exploited in computations for a different theory: in fact, introducing some modification in the defining Feynman rules, all subsequent results are affected. In the string approach, the situation is different: the basic ingredients of all calculations always arise from quantities defined on the string world-sheet, and thus are not dependent on the specific definition of the field theory limit one may consider. In particular, the building blocks are the measure of integration over string moduli and the Laplacian Green function on the string world-sheet, essentially the two-point correlator of two-dimensional scalar fields. This means that a large fraction of the calculation is done in a general framework, without specifying which states will be selected by the field theory limit. All these results can then be exploited for deriving different amplitudes in a given field theory, or even for calculations applying to different field theories. For instance, the number of external particles does not play such dramatic role in determining the complexity of the calculation. As we will show explicitly in the two-loop case, one can learn many informations about the shape of the relevant string world-sheets by studying simple vacuum bubble diagrams. The results obtained in this way will not be modified by the insertion of external legs. Similarly, there are relations among calculations in different theories; in fact, one chooses a specific field theory only when one selects, in the string master formula, the contributions of a specific state. Technically this step simply amounts to a Taylor expansion of all functions appearing in the string amplitude, keeping the appropriate powers of the variables describing the string world-sheet. Clearly, the building blocks of the calculation are not modified by changing the string state one focuses on; also, the overall normalization and the integration region over string moduli are fixed once and for all. In general, this unifying way of treating amplitudes of different theories brings many simplifications; for instance, the tensor algebra associated with the propagation of spin-1 (or spin-2) particles is bypassed, and the computational complexity of these amplitudes is almost reduced to that of scalar amplitudes.

Despite all the advantages just described, so far the technique has been fully applied only to massive scalars and to massless gauge bosons and gravitons, and has been completely successful only at one loop. There are several technical reasons for this limitation: the extension to fermions requires in principle the use of superstring amplitudes, and the multiloop technology in that case has not yet been completely developed; the extension to massive particles with spin is in principle possible, however one should realize that string theory is clearly ill-equipped to reproduce field theories with several mass scales, since all scales at the string level are proportional to the string tension T ; finally, the extension to two and more loops

has proven harder than expected, because it requires a detailed understanding of the multiloop string moduli space, whose corners contributing to the field theory limit manage to reconstruct the particle amplitudes in a highly non-trivial way. The present paper is a step towards the solution of the problems connected with the application of string techniques to multiloop diagrams. In particular, we study the two-loop open string moduli space, determine the correct integration region over moduli and punctures in the field theory limit, and show how different corners of moduli space cooperate to reconstruct individual Feynman diagrams, with the correct symmetry and color factors.

In this paper we focus on the study of scalar interactions. This means that both for external and for propagating states we will select the contributions coming from the open string tachyon, a Lorentz scalar taking values in the adjoint representation of the Chan-Paton group, which we shall take to be $U(N)$. In Section 2 we will introduce the technical tools needed for the computation of bosonic string amplitudes, and the Schottky parametrization of the string world-sheet. In Section 3 we will show how one can define two different point-particle limits, by matching in different ways the field coupling constant g , which is kept fixed when $\alpha' \rightarrow 0$, to the unique string coupling g_S . The two matchings lead to a cubic scalar interaction in $d = 6 - 2\epsilon$, and to a quartic scalar interaction in $d = 4 - 2\epsilon$, respectively. Each field theory arises naturally in the space-time dimension in which it is renormalizable, essentially because the string scale in the intermediate stages plays the role of a renormalization scale, and disappears from the matching conditions when the field coupling becomes dimensionless. As a first check, some tree-level amplitudes are derived from the string master formula. In Section 4 we turn to one-loop diagrams, which are fairly straightforward to handle, and thus serve as a useful preliminary to two-loop calculations. We give explicit expressions for multi-leg one-particle-irreducible diagrams both for cubic and quartic interactions, and we show how non-planar color structures (subleading in the large- N limit) are correctly reproduced in the string framework. Finally, in Section 5, we turn to the more challenging problem of two-loop diagrams. Different calculations are presented, up to the four-point amplitude, both for cubic and quartic interactions. We present a detailed analysis of the two-loop moduli space in the field theory limit, which leads us to recover the correct results *including* the normalization factors¹. Indeed, it appears clear that for these more complicated diagrams the color decomposition and the combinatoric coefficients are obtained more easily from the string approach than from usual field theory techniques. In Section 6 we present our conclusions, and our current assessment of the status of our method.

¹A different method to identify the regions of moduli space corresponding to two-loop quartic interactions, and to compute the corresponding amplitudes, has recently been introduced in Ref. ([34]).

2 Multiloop scalar amplitudes in string theory

As we have already anticipated, in bosonic string theory it is possible to write in a compact form a generic loop amplitude among string states, with an arbitrary number of loops and external legs. This formula can be immediately specialized to the case where all external states are scalars. The full, normalized, h -loop scattering amplitude [19] of M tachyons with momenta p_1, \dots, p_M , can be written as

$$\begin{aligned}
 A_M^{(h)}(p_1, \dots, p_M) &= \prod_{r=1}^{h+1} \left(\text{Tr} (\lambda^{a_1^r} \dots \lambda^{a_{N_r}^r}) \right) \frac{2^M g_S^{M+2h-2}}{(2\pi)^{dh}} (2\alpha')^{(Md-2M-2d)/4} \\
 &\times \int [dm]_h^M \prod_{i < j} \left[\frac{\exp \left(\mathcal{G}_{r_i, r_j}^{(h)}(z_i, z_j) \right)}{\sqrt{V_i'(0) V_j'(0)}} \right]^{2\alpha' p_i \cdot p_j} . \quad (2.1)
 \end{aligned}$$

Here g_S is the dimensionless string coupling constant, and the product of traces is the appropriate $U(N)$ Chan–Paton factor for a generic h -loop diagram with $h + 1$ boundaries labelled by the index r . In the planar case it becomes simply $N^h \text{Tr}(\lambda^{a_1} \dots \lambda^{a_M})$. $\mathcal{G}_{r_i, r_j}^{(h)}$ is the correlator of two world-sheet bosons located at z_i on the boundary labelled r_i , and at z_j on the boundary r_j , while $[dm]_h^M$ is the measure of integration over moduli space for an open Riemann surface with h loops and M punctures. Notice that since we consider $U(N)$ as a gauge group, we have to take into account only string amplitudes with oriented world-sheets; thus non-planar diagrams arise only when loops are formed by sewing together two non-consecutive punctures. Here we will not be interested in the exact expression of the geometric objects appearing in Eq. (2.1), which can be found in [35]; rather, we will focus on their general features, in order to emphasize the properties which play a crucial role in the field theory limit. For a more complete presentation of the mathematical tools we will briefly describe here, we refer to Ref. [35]. As is well known, the Schottky parametrization is particularly suited for the study of the field theory limit, so we will work always within this framework. In Fig. 3, in Section 4, and Fig. 6, in Section 5, we present the one- and the two-loop string world-sheets in the Schottky representation. It is easy to see how the idea of adding loops is implemented in this formalism. One starts from the upper half complex plane (equivalent to the disk, representing the tree-level scattering amplitude), and adds two circles with the same radius and with centers on the real axis, which must then be identified via a projective transformation. Each loop is thus characterized by three real parameters: the positions of the two centers on the real axis, and the radius of the circles, which fix respectively the position and the width of the holes added to the surface. The positions of the various circles are related to the fixed points of the projective transformations under which the pairs of circles are identified, usually denoted by ξ_μ and η_μ , ($\mu = 1, \dots, h$), while the width of the holes is determined by the third parameter characterizing the projective transformation, the multiplier k_μ . It is possible to use the projective invariance of string theory to

fix the location of up to three of the punctures z_i , or of the fixed points, but one cannot fix the multipliers, which in fact drive the field theory limit. In general, it is convenient to fix, say, two ξ 's and one η , except in the one-loop case, where one has only two fixed points; in this case one also specifies the position of one of the punctures. In the field theory limit, the surface must degenerate into a graph, and all massive string modes must decouple. One can show in general [18] that the relevant region of string moduli space is the region $k_\mu \rightarrow 0$, and furthermore the Taylor expansion of the integrand of the string amplitude in powers of the multipliers corresponds to a sum over the mass levels of the states circulating in the loops. Thus, for the field theory limit of scalar amplitudes, we can always ignore all higher powers in the multipliers. In this limit, the integration measure in Eq. (2.1) reads

$$[dm]_h^M = \Delta(\rho_a, \rho_b, \rho_c) \prod_{\mu=1}^h \left[\frac{dk_\mu d\xi_\mu d\eta_\mu}{k_\mu^2 (\xi_\mu - \eta_\mu)^2} \right] [\det(-i\tau_{\mu\nu})]^{-d/2} \left(\prod_{i=1}^M \frac{dz_i}{V_i'(0)} \right), \quad (2.2)$$

where the factor $\Delta(\rho_a, \rho_b, \rho_c)$ is the Faddeev–Popov determinant associated with the fixing of the overall projective invariance, and $\tau_{\mu\nu}$ is the period matrix of the surface, whose explicit values at one and two loops will be given in Eqs. (4.6) and (5.7) below. Note that all the dependence on the external states is concentrated in the last term. The factors of $V_i'(0)$ originate from the need to introduce local coordinates on the surface, $V_i(z)$, around each puncture, in order to perform the sewing procedure. Before discussing their role, let us introduce explicit expressions for the Green functions we will need. Also in this case, we report here just the leading term in the Taylor expansion in the multipliers (see [35] for the complete string expressions). At one loop, if the two punctures are on the same boundary, one finds [15]

$$\mathcal{G}^{(1)}(z_i, z_j) = \log|z_i - z_j| + \frac{1}{2 \log k} \log^2 \frac{z_i}{z_j}, \quad (2.3)$$

otherwise one has to use the “non-planar” Green function

$$\mathcal{G}_{NP}^{(1)}(z_i, z_j) = \log|z_i + z_j| + \frac{1}{2 \log k} \log^2 \frac{|z_i|}{|z_j|}. \quad (2.4)$$

Notice that in Eqs. (2.3) and (2.4) we have already chosen the projective gauge $\eta = 0$ and $\xi \rightarrow \infty$, so that only the multiplier k appears explicitly. At two loops the bosonic Green function becomes a little more complicated because one has to deal with a non-trivial dependence on the moduli of the two holes. In the planar case

$$\begin{aligned} \mathcal{G}^{(2)}(z_1, z_2) &= \log|z_1 - z_2| + \frac{1}{2} \left[\log k_1 \log k_2 - \log^2 S \right]^{-1} \\ &\times \left[\log^2 T \log k_2 + \log^2 U \log k_1 - 2 \log T \log U \log S \right]. \end{aligned} \quad (2.5)$$

The Green function now depends on two different multipliers and on four fixed points through the anharmonic ratios

$$\begin{aligned}
S &= \frac{(\eta_1 - \eta_2)(\xi_1 - \xi_2)}{(\xi_1 - \eta_2)(\eta_1 - \xi_2)} , \\
T &= \frac{(z_2 - \eta_1)(z_1 - \xi_1)}{(z_2 - \xi_1)(z_1 - \eta_1)} , \\
U &= \frac{(z_2 - \eta_2)(z_1 - \xi_2)}{(z_1 - \eta_2)(z_2 - \xi_2)} .
\end{aligned}
\tag{2.6}$$

As was already noticed in [15], at one loop, these Green functions do not have the expected periodicity properties. This is not really surprising, since it is known that the factor $\exp[\mathcal{G}(z_i, z_j)]$ appearing in the master equation (2.1) has conformal weight $(-1/2, -1/2)$ in the two variables (z_i, z_j) and not zero. Thus to give a global definition to Eq. (2.1), one should multiply it by a function of conformal weight $(1/2, 1/2)$. This suggests that one can recover a well behaved geometric object if the local coordinates $V'_i(0)$ compensate for this problem by having conformal weight -1 . A natural choice is to define the $V'_i(0)$ by using the inverse of the abelian differentials, which are the only globally defined objects having conformal weight one. By following this idea one recovers at one loop the choice made in [15] where $V'_i(0) = \omega^{-1}(z_i) = z_i$, since, in this case, there is a unique abelian differential, $\omega(z) = 1/z$. At two loops, one is led to identify the inverse of $V'_i(0)$ with a linear combination of the two differentials $\omega_1(z_i)$ and $\omega_2(z_i)$; to fix the normalization, we will follow Ref. [21], and require that this linear combination be normalized to one when one integrates it around the field theory propagator on which the leg is inserted. This is sufficient to fix the local coordinates for the purpose of the scalar field theory limit.

The string expressions reported here contain just the leading order in the multipliers; moreover, as we anticipated in the Introduction, in order to derive the field theory limit of Eq. (2.1), one has to Taylor expand the integrand also in all other variables. The logarithmic terms, however, are non-analytic and must have a special status. In fact, it turns out that they measure the length of field theory propagators in units of α' , and so are directly related to the Schwinger proper times of the limiting field theory. This means that, technically, the zero-slope limit has to be taken after introducing the field theory variables that have to be kept fixed: the string coupling constant has to be translated to the appropriate field theory coupling, while the logarithmic terms in the integrand must be interpreted in terms of proper times, in general as $\ln(x) \propto t/\alpha'$. The exact form of this change of integration variables depends on the particular corner of moduli space considered, as we will see in detail in the following sections.

Even if we gave explicit expressions for all functions entering in Eq. (2.1), our master formula is still a formal expression, since we have not yet specified the exact region of integration of the various parameters. We do not attempt to solve

this problem in its most general form; however, in the following sections, we will determine the correct region of integration, at least in the field theory limit, for the one- and two-loop diagrams. Here we just anticipate the basic idea. One starts considering the vacuum amplitudes, where it is possible to focus only on the world-sheet shape, without having to consider external punctures. In this way one determines the region of integrations over the fixed points, by requiring that the surface never become singular; on the other hand, the integration over the multipliers is fixed by symmetry arguments and is chosen in order to avoid double counting of equivalent configurations. When external legs are added, this setup is not essentially modified. From this analysis of the string world-sheet one can draw a clear representation of the various boundaries of the surface, and the punctures can take all possible values on these boundaries.

3 Tree-level matching conditions

We begin our analysis of the field theory limit by establishing the relationships between the string coupling and the couplings of the cubic and quartic theories we want to reproduce. This is done, as in effective field theory, by computing the simplest amplitudes both with strings and fields, and matching the results. The string amplitude is, of course, uniquely defined: different matchings correspond to different ways of taking the infinite tension limit, and they lead to different field theories in different dimensions. Having established the connection between the couplings, we go on to describe the computation of simple tree diagrams, with up to six external legs.

The on-shell, tree-level, color-ordered, M -point scalar amplitude in bosonic string theory is readily derived from Eq. (2.1), by choosing as Green function simply $\mathcal{G}(z_i, z_j) = \ln|z_i - z_j|$. The result is the correctly normalized Koba-Nielsen amplitude,

$$A_M^{(0)}(p_1, \dots, p_M) = \text{Tr}(\lambda^{a_1} \dots \lambda^{a_M}) 2^M g_S^{M-2} (2\alpha')^{(Md-2M-2d)/4} \times \int \prod_{i=1}^M dz_i \Delta(z_a, z_b, z_c) \prod_{i<j} (z_i - z_j)^{2\alpha' p_i \cdot p_j} . \quad (3.1)$$

Here the punctures z_i are ordered on a circle, as in the trace, and $\Delta(z_a, z_b, z_c)$ is the Faddeev-Popov determinant arising from the fixing of projective invariance,

$$\Delta(z_a, z_b, z_c) = \delta(z_a - z_a^{(0)}) \delta(z_b - z_b^{(0)}) \delta(z_c - z_c^{(0)}) (z_a - z_b)(z_a - z_c)(z_b - z_c) , \quad (3.2)$$

where $z_{a,b,c}$ are three arbitrarily chosen punctures whose location is fixed. In the present section we will always choose $z_1 \rightarrow \infty$, $z_2 = 1$ and $z_M = 0$, so that all remaining integrals range between 0 and 1.

With these choices, the 3–point amplitude is simply

$$A_3^{(0)}(p_1, p_2, p_3) = \text{Tr}(\lambda^{a_1} \lambda^{a_2} \lambda^{a_3}) 8g_S (2\alpha')^{(d-6)/4} , \quad (3.3)$$

whereas the 4–point amplitude (contributing to the Veneziano formula) is given by

$$\begin{aligned} A_4^{(0)}(p_1, p_2, p_3, p_4) &= \text{Tr}(\lambda^{a_1} \lambda^{a_2} \lambda^{a_3} \lambda^{a_4}) 16g_S^2 (2\alpha')^{(d-4)/2} \\ &\times \int_0^1 dz z^{2\alpha' p_3 \cdot p_4} (1-z)^{2\alpha' p_2 \cdot p_3} . \end{aligned} \quad (3.4)$$

Since we wish to consider a slightly more complicated example, we also give the expression for the 6–point function,

$$\begin{aligned} A_6^{(0)}(p_1, \dots, p_6) &= \text{Tr}(\lambda^{a_1} \dots \lambda^{a_6}) 64g_S^4 (2\alpha')^{(d-3)} \int_0^1 dz_3 \int_0^{z_3} dz_4 \int_0^{z_4} dz_5 \\ &\times \left[(1-z_3)^{2\alpha' p_2 \cdot p_3} (1-z_4)^{2\alpha' p_2 \cdot p_4} (1-z_5)^{2\alpha' p_2 \cdot p_5} (z_3-z_4)^{2\alpha' p_3 \cdot p_4} \right. \\ &\times \left. (z_3-z_5)^{2\alpha' p_3 \cdot p_5} (z_4-z_5)^{2\alpha' p_4 \cdot p_5} z_3^{2\alpha' p_3 \cdot p_6} z_4^{2\alpha' p_4 \cdot p_6} z_5^{2\alpha' p_5 \cdot p_6} \right] . \end{aligned} \quad (3.5)$$

Turning to field theory, let us first consider a scalar $U(N)$ theory defined by the lagrangian²

$$\mathcal{L}_3 = \text{Tr} \left[\partial_\mu \Phi \partial^\mu \Phi - m^2 \Phi^2 + \frac{2}{3} g_3 \Phi^3 \right] , \quad (3.6)$$

where $\Phi = \phi_\alpha \lambda^\alpha$ is a scalar field taking values in the adjoint representation of $U(N)$, and our generators are normalized by $\text{Tr}(\lambda_\alpha \lambda_\beta) = \delta_{\alpha\beta}/2$. Feynman rules for scalar $U(N)$ theories and several useful formulas for color structures are collected in the Appendix. The color–ordered 3–point amplitude (defined as $-i$ times the relevant Feynman diagram) in this theory is simply

$$A_3^{(0)}(p_1, p_2, p_3) = 2g_3 \text{Tr}(\lambda^{a_1} \lambda^{a_2} \lambda^{a_3}) . \quad (3.7)$$

Comparison with Eq. (3.3) yields the matching condition

$$g_3 = 4g_S (2\alpha')^{(d-6)/4} , \quad (3.8)$$

already derived in [19]. Note that the coupling is dimensionless in $d = 6$, as it must. We can now use Eq. (3.8) to compute higher order scattering amplitudes in the theory defined by Eq. (3.6), using the string master formula. As a first simple example, consider the 4–point amplitude, which becomes

$$\begin{aligned} A_4^{(0)}(p_1, \dots, p_4) &= \text{Tr}(\lambda^{a_1} \dots \lambda^{a_4}) 2g_3^2 \alpha' \\ &\times \int_0^1 dz z^{2\alpha' p_3 \cdot p_4} (1-z)^{2\alpha' p_2 \cdot p_3} . \end{aligned} \quad (3.9)$$

²Note that here we use a convention slightly different from the one employed in Ref. [19]; in particular we choose a coupling constant g_3 which is four times bigger than the one of [19], in order to reduce the number of factors of two in the amplitudes.

To get a sensible zero slope limit we must extract from the integral a factor $(\alpha')^{-1}$, which can be done by focusing on the potentially singular regions $z \rightarrow 0$ and $z \rightarrow 1$, corresponding to s - and t -channel exchange respectively (the u -channel diagram cannot contribute to this color structure). According to the general discussion of Section 2, and considering the region $z \rightarrow 0$, we do this by setting $z = \exp(-t_z/\alpha')$, with t_z finite and $\alpha' \rightarrow 0$. Neglecting $O(\alpha')$ corrections, the change of variables yields

$$\begin{aligned} A_4^{(0)}(p_1, \dots, p_4) &= \text{Tr}(\lambda^{a_1} \dots \lambda^{a_4}) 2g_3^2 \int_0^\infty dt_z \exp\left[-\frac{t_z}{\alpha'}(1 + 2\alpha' p_3 \cdot p_4)\right] \\ &= 2g_3^2 \text{Tr}(\lambda^{a_1} \dots \lambda^{a_4}) \frac{1}{(p_3 + p_4)^2 + m^2} \ , \end{aligned} \quad (3.10)$$

where we made use of the mass-shell condition $m^2 = -1/\alpha'$. Taking into account the similar contribution arising from the region $z \rightarrow 1$, we get the complete answer for this color ordering,

$$A_4^{(0)}(p_1, \dots, p_4) = 2g_3^2 \text{Tr}(\lambda^{a_1} \dots \lambda^{a_4}) \left[\frac{1}{(p_3 + p_4)^2 + m^2} + \frac{1}{(p_2 + p_3)^2 + m^2} \right] \ , \quad (3.11)$$

which exactly matches the correct result in field theory, provided the string metric is used.

It is clear that the different diagrams contributing to a given color ordering arise from different corners of string moduli space, and they are easily identified by the pole structure of their propagators. To illustrate this in a slightly less trivial configuration, let us consider the 6-point amplitude in Eq. (3.5), and let us attempt to separate the contributions to two different given diagrams, say those portrayed in Fig. 1. Using the matching condition, Eq. (3.8), one easily sees that

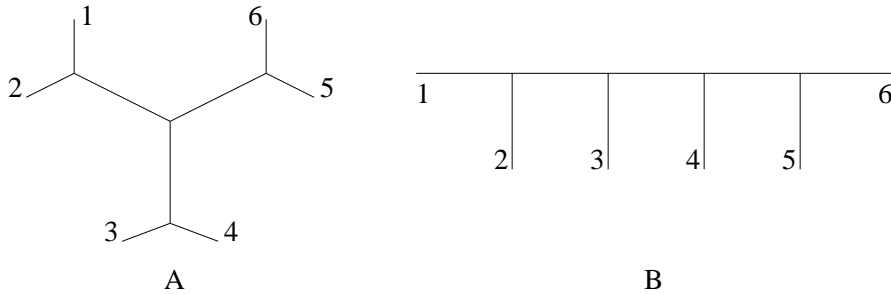


Figure 1: Two tree-level six-point diagrams with cubic vertices.

the string amplitude is proportional to $(\alpha')^3$, so that we need to take a limit in all three integration variables, which corresponds to the extraction of three propagator poles. If we want to specify the region in moduli space relevant for diagram A, we must qualitatively have z_5 very close to $z_6 = 0$, and z_3 very close to z_4 . Moreover the

three pairs of variables (z_1, z_2) , (z_3, z_4) and (z_5, z_6) have to be kept widely separated from each other. The desired change of variables is

$$\begin{aligned} z_3 &= e^{-t_3/\alpha'} \\ z_3 - z_4 &= e^{-t_4/\alpha'} \\ z_5 &= e^{-t_5/\alpha'} \quad . \end{aligned} \tag{3.12}$$

In terms of these ‘‘proper times’’, and neglecting terms suppressed by powers of α' , the amplitude reads

$$\begin{aligned} A_6^{(0)}(p_1, \dots, p_6) &= \text{Tr}(\lambda^{a_1} \dots \lambda^{a_6}) 2g_3^4 \int_0^\infty dt_3 \int_{t_3}^\infty dt_4 \int_{t_3}^\infty dt_5 \\ &\times \exp\left[-\frac{t_4}{\alpha'}(1 + 2\alpha' p_3 \cdot p_4)\right] \exp\left[-\frac{t_5}{\alpha'}(1 + 2\alpha' p_5 \cdot p_6)\right] \\ &\times \exp\left[-\frac{t_3}{\alpha'}(1 + 2\alpha' p_3 \cdot p_5 + 2\alpha' p_3 \cdot p_6 + 2\alpha' p_4 \cdot p_5 + 2\alpha' p_4 \cdot p_6)\right] \quad . \end{aligned} \tag{3.13}$$

One easily sees that the contribution of this region to the 6-point amplitude is

$$A_6^{(0)} = \text{Tr}(\lambda^{a_1} \dots \lambda^{a_6}) 2g_3^4 \frac{1}{(p_1 + p_2)^2 + m^2} \frac{1}{(p_3 + p_4)^2 + m^2} \frac{1}{(p_5 + p_6)^2 + m^2} \quad , \tag{3.14}$$

precisely the desired result.

For the other diagram of Fig. 1, one has to consider a different change of variables; in particular, since now we do not want to group external particles in pairs, all z_i 's must be taken widely separated. Thus the corresponding ‘‘ordered proper times’’ are simply defined as $t_i = -\alpha' \ln z_i$. Following the same steps just described, it is the easy to check that the expected result for diagram B is obtained. We note in passing that finding the numerical coefficient of a given color ordering for a given Feynman diagram may be a rather cumbersome task with the conventional Feynman rules, whereas it is immediate here.

Let us now turn our attention to quartic interactions. We want to reconstruct the amplitudes derived from the lagrangian

$$\mathcal{L}_4 = \text{Tr} \left[\partial_\mu \Phi \partial^\mu \Phi - m^2 \Phi^2 + g_4 \Phi^4 \right] \quad , \tag{3.15}$$

which, in particular, yields the color-ordered vertex

$$A_4^{(0)}(p_1, p_2, p_3, p_4) = 4g_4 \text{Tr}(\lambda^{a_1} \lambda^{a_2} \lambda^{a_3} \lambda^{a_4}) \quad . \tag{3.16}$$

The starting point is now Eq. (3.4), where however in this case we do not need to generate any extra powers of α' , as was done to go from Eq. (3.9) to Eq. (3.10). Here the overall dimensionality is correct, so all we need to do is take the $\alpha' \rightarrow 0$ limit and integrate over z without introducing any weight in special corners of moduli space. In other words, the quartic vertex arises from integration over finite regions

of moduli space, and not from its boundaries (regions of infinitesimal size in the field theory limit). As $\alpha' \rightarrow 0$, the integrand of Eq. (3.4) simply becomes 1, so we get

$$A_4^{(0)}(p_1, p_2, p_3, p_4) = 16g_S^2 (2\alpha')^{(d-4)/2} \text{Tr}(\lambda^{a_1} \lambda^{a_2} \lambda^{a_3} \lambda^{a_4}) \quad . \quad (3.17)$$

Comparison with Eq. (3.16) yields the matching condition

$$g_4 = 4g_S^2 (2\alpha')^{(d-4)/2} \quad . \quad (3.18)$$

The same matching condition might have been obtained in a different way, by first considering the Φ^3 diagrams contributing to $A_4^{(0)}$, and then explicitly deleting the internal propagators by setting their proper times to 0, inserting in turn a $\delta(t_z/\alpha')$ and a $\delta((t - t_z)/\alpha')$. These δ functions should however be regularized, since they are located at the boundaries of the integration region. In such circumstances it is natural to weigh each δ function with a factor 1/2, and this reproduces the matching in Eq. (3.18). This second method is closer in spirit to the techniques of [34].

To show that this procedure can be generalized to higher order amplitudes, let us consider also for Φ^4 a particular diagram contributing to the 6-point amplitude. Note that there are 105 diagrams contributing to the Φ^3 6-point amplitude, but only 10 with quartic vertices. We consider, as an example, the diagram depicted in Fig. 2. Using the matching condition Eq. (3.18) in the string amplitude, Eq. (3.5),

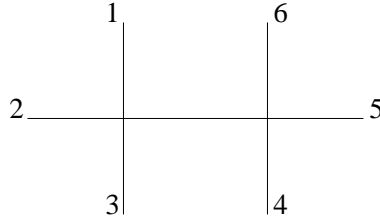


Figure 2: A sample tree-level six-point diagram with quartic vertices.

one sees that the amplitude has an overall factor of α' . Thus we need to take precisely one singular limit in one of the integration variables, corresponding to the extraction of a single propagator pole. For the particular diagram at hand, qualitatively, we would like to keep z_4 and z_5 close to $z_6 = 0$, while leaving z_3 close to 1. This can be achieved by the change of variables

$$\begin{aligned} z_3 &= x \\ z_4 &= e^{-t_4/\alpha'} \\ z_5 &= y e^{-t_4/\alpha'} \quad , \end{aligned} \quad (3.19)$$

with no proper times associated with x and y . Neglecting as usual terms suppressed by powers of α' , we get

$$A_6^{(0)}(p_1, \dots, p_6) = \text{Tr}(\lambda^{a_1} \dots \lambda^{a_6}) 8g_4^2 \int_0^1 dx \int_0^1 dy \int_0^\infty dt_4$$

$$\begin{aligned}
& \exp \left[-\frac{t_4}{\alpha'} (2 + 2\alpha' p_4 \cdot p_5 + 2\alpha' p_4 \cdot p_6 + 2\alpha' p_5 \cdot p_6) \right] \\
&= \text{Tr} (\lambda^{a_1} \dots \lambda^{a_6}) 8g_4^2 \frac{1}{(p_4 + p_5 + p_6)^2 + m^2} . \quad (3.20)
\end{aligned}$$

Once again, the computation of the color factor of the corresponding Feynman diagram yields the same result.

4 One-loop diagrams

The multi-tachyon planar one-loop amplitude derived from Eq. (2.1) can be written as

$$\begin{aligned}
A_M^{(1)}(p_1, \dots, p_M) &= N \text{Tr}(\lambda^{a_1} \dots \lambda^{a_M}) \frac{1}{(4\pi)^{d/2}} 2^M g_S^M (2\alpha')^{(Md-2M-2d)/4} \\
&\times \int_0^1 \frac{dk}{k^2} \left(-\frac{\log k}{2} \right)^{-d/2} \int_k^1 dz_2 \int_k^{z_2} dz_3 \dots \int_k^{z_{M-1}} dz_M \\
&\times \prod_{i=1}^M \frac{1}{V_i'(0)} \prod_{i<j} \left[\frac{\exp(\mathcal{G}^{(1)}(z_i, z_j))}{\sqrt{V_i'(0) V_j'(0)}} \right]^{2\alpha' p_i \cdot p_j} , \quad (4.1)
\end{aligned}$$

where we neglected $O(k)$ terms in the measure of integration that will not contribute to the field theory limit, and we have introduced the local coordinates $V_i(z)$, according to the general discussion of Section 2. Projective invariance has been used to choose the fixed points of the single Schottky generator as $\eta = 0$ and $\xi \rightarrow \infty$, and to fix $z_1 = 1$. In this configuration the world-sheet of the string (an annulus) can be represented as in Fig. 3. For a planar configuration, all punctures are constrained

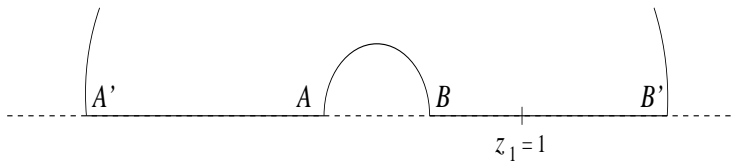


Figure 3: The annulus in the Schottky representation.

to lie on the same boundary of the string world sheet, thus, having fixed $z_1 = 1$, all other z_i should be integrated over the interval $B = \sqrt{k} < z_i < B' = 1/\sqrt{k}$, with the restriction on the ordering implied by the color trace. This would complicate the calculation of the field theory limit, since there would be contributions both from $z_i \rightarrow \sqrt{k} \rightarrow 0$ and from $z_i \rightarrow 1/\sqrt{k} \rightarrow \infty$. It is possible to bypass this practical difficulty by making use of the fact that the string integrand is modular

invariant, which in particular implies that the interval $[1, 1/\sqrt{k}]$ can be mapped onto the interval $[k, \sqrt{k}]$. In fact, defining the effective one-loop Green function by

$$G^{(1)}(z_i, z_j; k) = \mathcal{G}^{(1)}(z_i, z_j) - \frac{1}{2} \log V_i'(0) - \frac{1}{2} \log V_j'(0) \quad , \quad (4.2)$$

and choosing $V_i'(0) = z_i$, according to our general discussion, it is easy to check that the effective Green function at the string level is a function only of the ratio $\rho_{ij} = z_i/z_j$, and satisfies

$$\begin{aligned} G^{(1)}(\rho_{ji}, k) &= G^{(1)}(\rho_{ij}, k) \\ G^{(1)}(k\rho_{ji}, k) &= G^{(1)}(\rho_{ij}, k) \quad . \end{aligned} \quad (4.3)$$

Using these properties, one can map all configurations with a subset of punctures in the interval $[1, 1/\sqrt{k}]$ to configurations in which those punctures have been moved to the interval $[k, \sqrt{k}]$, preserving the ordering on the circle. This procedure yields the integration region in Eq. (4.1). In the field theory ($k \rightarrow 0$) limit the effective Green function has the form

$$G^{(1)}(z_i, z_j; k) = \log \left(\sqrt{\frac{z_i}{z_j}} - \sqrt{\frac{z_j}{z_i}} \right) + \frac{1}{2 \log k} \log^2 \frac{z_i}{z_j} \quad , \quad (4.4)$$

for $z_i > z_j$.

The generalization of Eq. (4.1) to the case of non-planar diagrams is known [36], and easily understood. A non planar diagram has punctures on both boundaries, so the factor of $N = \text{Tr} \mathbf{1}$ is replaced by the trace of the Chan-Paton factors corresponding to the punctures on the second boundary (the interval $[-1/\sqrt{k}, -\sqrt{k}]$ in Fig. 3). The region of integration of the corresponding z_i is an ordered region on the negative real axis. The string Green function involving two punctures on the negative real axis is precisely the same as the one discussed above, since it is a function only of the ratio ρ_{ij} , which remains positive when both z 's change sign. The only subtlety involves the Green function connecting punctures on different boundaries. In this case the terms in the Green function arising from loop momentum integration behave differently, and one should choose $V_i'(0) = |z_i|$, so that the Green function remains real, and does not have any singularity when $|z_i| \rightarrow |z_j|$. In the field theory limit one finds simply

$$G_{NP}^{(1)}(z_i, z_j; k) = \log \left(\sqrt{\frac{|z_i|}{|z_j|}} + \sqrt{\frac{|z_j|}{|z_i|}} \right) + \frac{1}{2 \log k} \log^2 \frac{|z_i|}{|z_j|} \quad , \quad (4.5)$$

where the two z 's have opposite signs.

4.1 One-loop cubic interactions

Armed with the appropriate string technology, let us examine how one-loop scalar diagrams with cubic interactions emerge from Eq. (4.1). Following [19], we begin by

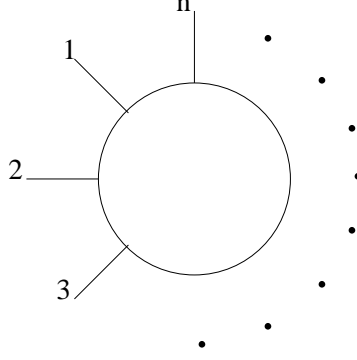


Figure 4: Multi-leg one-loop one-particle-irreducible diagram in a Φ^3 theory.

considering the general configuration of a one-loop one-particle-irreducible diagram with n external legs, depicted in Fig. 4. Using the matching condition Eq. (3.8), we find

$$\begin{aligned}
A_{n,1PI}^{(1)}(p_1, \dots, p_n) &= N \text{Tr}(\lambda^{a_1} \dots \lambda^{a_M}) \frac{g_3^n}{(4\pi)^{d/2}} (2\alpha')^{-d/2} (\alpha')^n \\
&\times \int_0^1 \frac{dk}{k^2} \left(-\frac{\log k}{2} \right)^{-d/2} \int_k^1 \frac{dz_2}{z_2} \int_k^{z_2} \frac{dz_3}{z_3} \dots \int_k^{z_{n-1}} \frac{dz_n}{z_n} \\
&\times \exp \left[\sum_{i < j} (2\alpha' p_i \cdot p_j G^{(1)}(z_i, z_j)) \right] . \tag{4.6}
\end{aligned}$$

As usual, the field theory limit is governed by the multiplier k , which must be taken to be exponentially suppressed as $\alpha' \rightarrow 0$, so that the length of the string loop may become infinite in units of α' . The tachyon double pole is regulated, as described in Ref. ([19]), by setting $dk/k^2 = \exp(m^2 \alpha' \log k) dk/k$. The appropriate change of variables is then

$$\begin{aligned}
k &= e^{-T/\alpha'} \\
z_i &= e^{-t_i/\alpha'} . \tag{4.7}
\end{aligned}$$

All puncture coordinates must become exponentially small as $\alpha' \rightarrow 0$, so that the correct power of α' may be generated. Defining the Feynman parameters as $x_i = t_{n+1-i}/T$, for $i = 1, \dots, n-1$, we find an expression which may easily be compared with the field-theoretic result,

$$\begin{aligned}
A_{n,1PI}^{(1)}(p_1, \dots, p_n) &= N \text{Tr}(\lambda^{a_1} \dots \lambda^{a_M}) \frac{g_3^n}{(4\pi)^{d/2}} \\
&\times \int_0^\infty dT T^{n-1-d/2} e^{-m^2 T} \int_0^1 dx_1 \int_0^{x_1} dx_2 \dots \int_0^{x_{n-2}} dx_{n-1} \\
&\times \exp \left[T \sum_{i < j} p_i \cdot p_j (x_{ij}(1 - x_{ij})) \right] , \tag{4.8}
\end{aligned}$$

where $x_{ij} = x_i - x_j$. We note in passing that deriving the coefficient of the leading color trace from the Feynman rules is not trivial for the general diagram with n legs. In fact, the above could be considered as a simple proof that the coefficient is N for any n . The expression for the integrand as a function of the parameters x_i also appears automatically in the most symmetric form; note that this is the correct form for arbitrary values of the external momenta p_i , on- or off-shell.

Before going on to perform a similar calculation for quartic interactions, it is worthwhile to pause to consider two instructive special cases of Eq. (4.8), and a slight generalization of it in the case of the four-point function. First of all we would like to point out that Eq. (4.8) holds in field theory for all n , including $n = 2$, because of what appears at first sight as a fortunate coincidence: in fact in field theory the color factor for the two point function is *twice* the one appearing in Eq. (4.8), essentially because $\text{Tr}(\lambda_a \lambda_b) = \text{Tr}(\lambda_b \lambda_a)$. However this factor of 2 is compensated by a symmetry factor of $1/2$, which is only present for the two-point amplitude. String theory takes into account these two facts simultaneously and automatically.

Another unexpected feature of the two-point function in field theory is the fact that, if one allows the external scalars to take values in the $U(1)$ factor of $U(N)$, that is if one allows the indices a, b to take the value 0, one finds that the color factor of the corresponding diagram doubles. This is easily seen from Eqs. (A.10) and (A.12), in the Appendix. This fact is unexplained from the point of view of Feynman diagrams, but it has a natural explanation in string theory. In fact, if in string theory we allow the external legs to be color singlets, the amplitude receives a contribution from a *new diagram*, the one with the two legs inserted on different world sheet boundaries. This diagram, which is non-planar from the point of view of string theory, contributes at the same order in N because with a correctly normalized $U(1)$ generator (see the Appendix) one finds that $\text{Tr}(\lambda_0^2) \text{Tr}(\mathbf{1}) = (\text{Tr}(\lambda_0))^2$. Furthermore, it is easy to check that the functional form of this new diagram is precisely the same as that of the original diagram, with the same overall factor and integration region. This is the first simple example of the correct handling of non-planar contribution in string theory.

We conclude this section by giving a further non-trivial example of a non-planar contribution to a one-loop amplitude. We consider the four-point function, which in field theory yields contributions proportional to double color traces, such as $\text{Tr}(\lambda_{a_1} \lambda_{a_4}) \text{Tr}(\lambda_{a_2} \lambda_{a_3})$. These double trace contributions naturally arise in string theory from the simultaneous insertion of punctures on the two different string boundaries. In field theory, on the other hand, these terms receive contributions from different Feynman diagrams. Choosing for example the cyclic order 1, 2, 3, 4 for the external legs, the complete color factor in field theory, is given by

$$\begin{aligned}
\mathcal{C}_{1234} &= N [\text{Tr}(\lambda^{a_1} \lambda^{a_2} \lambda^{a_3} \lambda^{a_4}) + \text{Tr}(\lambda^{a_4} \lambda^{a_3} \lambda^{a_2} \lambda^{a_1})] \\
&+ 2\text{Tr}(\lambda^{a_1} \lambda^{a_2}) \text{Tr}(\lambda^{a_3} \lambda^{a_4}) + 2\text{Tr}(\lambda^{a_1} \lambda^{a_3}) \text{Tr}(\lambda^{a_2} \lambda^{a_4}) \\
&+ 2\text{Tr}(\lambda^{a_1} \lambda^{a_4}) \text{Tr}(\lambda^{a_2} \lambda^{a_3}) \quad , \tag{4.9}
\end{aligned}$$

so that the coefficient of the chosen term is 2. One should keep in mind, however, that the particular color structure $\text{Tr}(\lambda^{a_1} \lambda^{a_4}) \text{Tr}(\lambda^{a_2} \lambda^{a_3})$ receives contributions also from two other distinct Feynman diagrams, corresponding to the non-cyclic permutations of the external particles in the original one (in the present case, the orderings 1, 3, 2, 4 and 1, 4, 2, 3). String theory must, and does, assemble the contributions of the different diagrams to the chosen color structure into a single string configuration. This can be verified by using the non-planar Green function Eq. (4.5), and considering all possible ways of inserting the punctures on the boundaries. Since we wish to place the puncture z_4 on the same boundary as $z_1 = 1$, it must lie on the positive real axis in Fig. 3. As explained above, this leads to the integration region $k \leq z_4 \leq 1$. For the other two punctures, on the negative axis, the integration region is $-1 \leq \{z_2, z_3\} \leq -k$, with no restriction on the relative ordering of z_2 and z_3 . Changing variables to $x_2 = -z_2$ and $x_3 = -z_3$, we have once again four punctures on the positive real axis, which can be placed in the interval $[k, z_1 = 1]$ in six different orderings. Note that the six orderings are distinguishable in the field theory limit, because the logarithmic term in the generic Green function has a different field theory limit depending on the ordering, $\log(z_i \pm z_j) \rightarrow \log(z_i)$, for $z_i > z_j$. An explicit calculation shows that the orderings $x_2 \leq x_3 \leq z_4$ and $z_4 \leq x_3 \leq x_2$ conspire to reconstruct the contribution to the chosen trace of the field theory diagram with cyclic ordering 1, 2, 3, 4, with the correct overall factor of 2. Similarly, the orderings $x_2 \leq z_4 \leq x_3$ and $x_3 \leq z_4 \leq x_2$ reconstruct the contribution of the diagram with cyclic ordering 1, 2, 4, 3, while the remaining two orderings give the last diagram. Once again, the building blocks of the final result are assembled in novel and non-trivial way.

4.2 One-loop quartic interactions

As in the previous section, it is possible to give a general expression for the one-loop, color-ordered, one-particle-irreducible diagram with n external legs, but only quartic vertices, shown in Fig. 5. Using the matching condition Eq. (3.18) in Eq. (4.1),

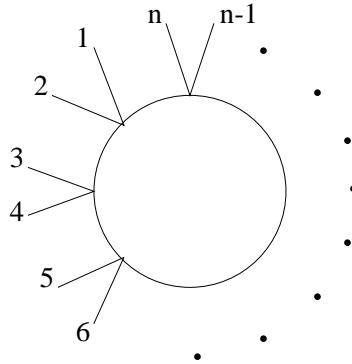


Figure 5: Multi-leg one-loop one-particle-irreducible diagram in a Φ^4 theory.

we get an expression very similar to Eq. (4.6),

$$\begin{aligned}
A_{n,1PI}^{(1)}(p_1, \dots, p_n) &= N \text{Tr}(\lambda^{a_1} \dots \lambda^{a_M}) \frac{g_4^{n/2}}{(4\pi)^{d/2}} (2\alpha')^{n/2-d/2} \\
&\times \int_0^1 \frac{dk}{k^2} \left(-\frac{\log k}{2} \right)^{-d/2} \int_k^1 \frac{dz_2}{z_2} \int_k^{z_2} \frac{dz_3}{z_3} \dots \int_k^{z_{n-1}} \frac{dz_n}{z_n} \\
&\times \exp \left[\sum_{i < j} \left(2\alpha' p_i \cdot p_j G^{(1)}(z_i, z_j) \right) \right] . \tag{4.10}
\end{aligned}$$

It is clear, however, that in this case we must introduce proper times for only one half of the integration variables, in order to compensate for the overall factor of $(\alpha')^{n/2}$. To obtain the configuration shown in Fig. 5, the appropriate change of variables is

$$\begin{aligned}
z_i &= e^{-t_i/\alpha'} , & (\text{i odd}) \\
z_i &= y_i z_{i-1} , & (\text{i even}) \\
k &= e^{-T/\alpha'} , &
\end{aligned} \tag{4.11}$$

with no proper time associated to the variables y_i and, as usual, $z_1 = 1$. Using Eq. (4.11) and neglecting terms suppressed as $\alpha' \rightarrow 0$, one gets

$$\begin{aligned}
A_{n,1PI}^{(1)}(p_1, \dots, p_n) &= N \text{Tr}(\lambda^{a_1} \dots \lambda^{a_M}) \frac{(2g_4)^{n/2}}{(4\pi)^{d/2}} \\
&\times \int_0^\infty dT T^{-d/2} e^{-m^2 T} \int_0^1 \frac{dy_2}{y_2} \int_0^T dt_3 \dots \int_0^{t_{n-3}} dt_{n-1} \int_0^1 \frac{dy_n}{y_n} \\
&\times \exp \left[\sum_{i < j \text{ odd}} (p_i + p_{i+1}) \cdot (p_j + p_{j+1}) \left(t_j - t_i - \frac{(t_j - t_i)^2}{T} \right) \right] . \tag{4.12}
\end{aligned}$$

The integrals in dy_i , ranging over finite regions of moduli space, are logarithmically divergent and need to be regularized. This divergence is actually a further manifestation of the tachyonic nature of the bosonic string ground state, and must be dealt with by the same method used to handle the double pole dk/k^2 : one must substitute $y_i^{-1} \rightarrow \exp(m^2 \alpha' \log y_i)$. In this case, however, there is no proper time associated with y_i so the exponential factors are suppressed as $\alpha' \rightarrow 0$ and must be neglected. The product of all dy_i integrals then yields simply a factor of unity. This procedure can be further justified by noting that the factors of y_i^{-1} arise from the factors $(V_i'(0))^{-1}$ in Eq. (4.1), which are characteristic of tachyon propagation and are absent, for example, in gluon amplitudes. In fact Eq. (4.1) can be continued consistently to an arbitrary value of the string intercept $a = -m^2 \alpha' \neq 1$, as was done in [37]. In that case one finds that the measure of integration changes as $dk/(k^2 \prod_i V_i'(0)) \rightarrow (dk/k)(k \prod_i V_i'(0))^{-a}$, indicating that the singularities generated by the projective transformations $V_i'(0)$ are of the same type as the double pole in the multiplier k .

With this regularization and changing variables to $x_i = 1 - t_i/T$, we find the simple formula

$$\begin{aligned}
A_{n,1PI}^{(1)}(p_1, \dots, p_n) &= 2^{n/2} N \operatorname{Tr}(\lambda^{a_1} \dots \lambda^{a_M}) \frac{g_4^{n/2}}{(4\pi)^{d/2}} \\
&\times \int_0^\infty dT T^{(n-2-d)/2} e^{-m^2 T} \int_0^1 dx_3 \int_0^{x_3} dx_5 \dots \int_0^{x_{n-3}} dx_{n-1} \\
&\times \exp \left[T \sum_{i < j \text{ odd}} (p_i + p_{i+1}) \cdot (p_j + p_{j+1}) (x_{ij}(1 - x_{ij})) \right].
\end{aligned} \tag{4.13}$$

Once again, this matches the result arising from the Feynman diagram in Fig. 5, with the restriction that paired external legs must not be of the same color. This provides a simple proof of the fact that for such diagrams the coefficient of the leading color trace is $2^{n/2}N$.

We conclude this section by noting a special case that arises in the computation of these loop amplitudes, when two consecutive external particles $((2n-1, 2n))$ annihilate in two colorless states running in the loop. Let us, for instance, focus on the special case of Eq. (4.13) where $n = 2$; this of course represents a tadpole diagram. For this diagram Eq. (4.13) yields

$$A_{2,1PI}^{(1)}(p_1, p_2) = 2 N \operatorname{Tr}(\lambda^a \lambda^b) \frac{g_4}{(4\pi)^{d/2}} \int_0^\infty dT T^{-d/2} e^{-m^2 T}, \tag{4.14}$$

which is one half of the result obtained in field theory. This discrepancy can be understood by observing that the color factor in field theory is of the form

$$\mathcal{C}_{ab} = 4 N \operatorname{Tr}(\lambda_a \lambda_b) = d_{ab\mu} d^{\mu\gamma}_\gamma + 2d_{a\mu\nu} d_b^{\mu\nu}. \tag{4.15}$$

The first contraction of d -tensors, which contributes one half of the total result, represents an ‘anomalous’ color flow corresponding to a Φ^3 tadpole diagram, in which the colored scalars a and $b = a$ annihilate into a color singlet state which then self-interacts. Clearly in this channel the full $U(N)$ color flow is prohibited, and only the $U(1)$ factor contributes. This term is missed by Eq. (4.13), but can be reproduced by first generating a one-particle-reducible Φ^3 diagram and then deleting the zero-momentum propagator, thus attaching the loop to the external legs. A similar peculiarity will arise when we will consider the two-loop Φ^4 vacuum bubbles, where also a tadpole-like configuration forcing the color flow to be restricted to $U(1)$ is present. This kind of term is always related to corners of moduli space corresponding to one-particle-reducible diagrams, and this is signaled by a color factor which displays a combinations of d_{abc} symbols typical of these diagrams.

5 Two-loop diagrams

Generalizing the approach described in the previous section to the two-loop case is not a straightforward task. First, the explicit expressions of the measure and of

the other geometrical objects present in Eq. (2.1) are more complex, so that the computation of physically interesting quantities (such as Yang–Mills amplitudes) has to be performed by means of a computer program. Second, there are also conceptual novelties, and the procedure described in the previous section cannot be applied directly to a two–loop calculation. Many of the new features are related to the fact that now the string world–sheet is a two–annulus and some of the simplifying choices that are usually made at one–loop are not possible any more. For example, in Eq. (4.1) the fixed points played no role, because they could be gauge–fixed to zero and infinity. In two–loop calculations, on the other hand, the shape of the string world–sheet can vary in a non–trivial manner. In fact, the measure Eq. (2.2) depends crucially on at least one of the fixed points, which means that the relative position of the two holes can not be fixed. Thus, for a better understanding of the new geometrical features, it is worthwhile to start the study of two–loop string amplitudes by considering in detail the Schottky parametrization, as it arises from the sewing procedure leading to Eq. (2.1). Basically, the two–loop surface can be constructed starting at one loop and identifying two external legs. This is done by cutting away from the one–loop string world–sheet two circles, and identifying their boundaries. If one chooses to sew together the puncture fixed at $z_1 = 1$ with one of the other legs on the same boundary (*i.e.* with $z_i > 0$ in order to construct a planar diagram), one obtains the two–loop surface depicted in Fig. 6.

We fix projective invariance by choosing $\eta_2 = 0$, $\xi_2 \rightarrow \infty$ and $\xi_1 = 1$. Then the positions and radii of the circles in Fig. 6 are completely determined as functions of the multipliers k_1 , k_2 and of the fixed point η_1 ; in fact, following [19], one can verify that

$$B = -A = \sqrt{k_2} \quad , \quad C = \frac{\eta_1 - \sqrt{k_1}}{1 - \sqrt{k_1}} \quad , \quad D = \frac{\eta_1 + \sqrt{k_1}}{1 + \sqrt{k_1}} \quad , \quad (5.1)$$

$$D' = \frac{1 + \eta_1 \sqrt{k_1}}{1 + \sqrt{k_1}} \quad , \quad C' = \frac{1 - \eta_1 \sqrt{k_1}}{1 - \sqrt{k_1}} \quad , \quad B' = -A' = \frac{1}{\sqrt{k_2}} \quad . \quad (5.2)$$

One can check that the points A , B , C and D are identified with A' , B' , C' and D' , respectively, under the action of the two generators of the two–loop Schottky group, *i.e.* the projective transformations mapping the circles $K_{1,2}$ into their images $K'_{1,2}$.

By cutting open a two–annulus, it is possible to map the two segments (AA') and (DD') onto the inner boundaries of the world–sheet, which is natural since their length depends only on k_1 and k_2 . Then the union of (BC) and $(C'B')$ represents the external boundary. Note that, in order to avoid a degenerate surface, the various identified circles should not overlap. This simple consideration gives a first constraint on the region of integration of the string moduli. In fact, by requiring that B does not touch C one obtains

$$\eta > \sqrt{k_1} + \sqrt{k_2} - \sqrt{k_1 k_2} \quad , \quad (5.3)$$

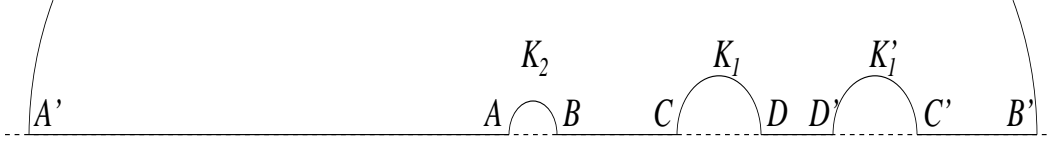


Figure 6: In the Schottky parametrization, the two-annulus corresponds to the part of the upper-half plane which is inside the big circle passing through A' and B' , and which is outside the circles K_1 , K_1' and K_2 .

while the same requirement on the segment (DD') leads to

$$D' - D = \frac{1 - \sqrt{k_1}}{1 + \sqrt{k_1}} (1 - \eta_1) \quad , \quad (5.4)$$

so that $\eta < 1$. Now the interpretation of the three moduli, k_1 , k_2 and η_1 , is particularly simple. In fact, $\sqrt{k_2}$ is the radius of the circle K_2 , while the radii of K_1 and K_1' are equal and depend on $\sqrt{k_1}$

$$R_{K_1} = \sqrt{k_1} \left(\frac{1 - \eta_1}{1 - k_1} \right) \quad . \quad (5.5)$$

Furthermore, η_1 turns out to be inside K_1 , while the point $\xi_1 = 1$ is inside K_1' . Therefore, in this configuration, the circle K_1' is fixed while K_1 can move, depending on the value of η_1 . In particular, if the point D' is very close to D , η_1 is almost equal to 1, while if C is near to B , then η_1 is of order of $\sqrt{k_1} + \sqrt{k_2}$. In other words, it is possible to interpret η_1 as the “distance” between the two loops. When $\eta_1 \rightarrow 1$, one may expect the field theory limit (at least for cubic interactions) to yield reducible diagrams with the two loops widely separated, while when $\eta_1 \rightarrow \sqrt{k_1} + \sqrt{k_2} \rightarrow 0$ one should obtain the irreducible diagrams with the two loops attached to each other.

Another observation relevant for deriving the region of integration of world-sheet moduli is that in the explicit form of all geometrical objects (for instance, the Green function or the measure) the multipliers k_1 and k_2 appear symmetrically, reflecting the equivalence of the two loops. Therefore, in order to avoid double counting of equivalent configurations, one can order the multipliers, by choosing for example $k_2 < k_1$. Note that the multipliers will always be associated with field theory proper times, so in the zero-slope limit their ordering should always be interpreted as strong ordering.

A final remark has to be made about the possibility of taking the attractive fixed point η bigger in modulus than the repulsive one ξ . As was shown in [38], in the closed string case these configurations are related to the one with $|\eta| < |\xi|$ by the residual part of the modular invariance group which survives in the field theory limit. In the open string case there is no modular invariance, but these surfaces should describe the propagation of closed string states, and they should not be included in our analysis. Thus, for our purposes, we will always restrict $|\eta|$ to be

less than $|\xi|$. Summarizing, we have found for k_1 , k_2 and η_1 , in the field theory limit, the same region of integration derived by Roland [38] for the closed string, *i.e.* $0 \leq \sqrt{k_2} < \sqrt{k_1} < |\eta_1| \leq 1$. We are now ready to move on to the evaluation of two-loop diagrams, starting with the simplest ones to verify our assumptions.

5.1 Vacuum bubbles

Let us start by briefly describing the simplest amplitude, the two-loop vacuum bubbles with cubic interaction. In this case ($M = 0$ and $h = 2$), with the projective gauge choice and integration region described above, and using the matching condition for cubic interaction, Eq. (3.8), Eq. (2.1) simply becomes

$$A_0^{(2)} = \frac{N^3}{(4\pi)^d} \frac{g_3^2}{16} (2\alpha')^{3-d} \int_0^1 \frac{d\eta_1}{(1-\eta_1)^2} \int_0^{\eta_1} \frac{dk_1}{k_1^2} \int_0^{k_1} \frac{dk_2}{k_2^2} \times \left[\frac{1}{4} (\log k_1 \log k_2 - \log^2 \eta_1) \right]^{-d/2}, \quad (5.6)$$

In Eq. (5.6) only the determinant of the period matrix is needed; at leading order in the two multipliers, it is

$$\det(-i\tau_{\mu\nu}) = \frac{1}{4\pi^2} \left[\log k_1 \log k_2 - \log^2 \eta \right]. \quad (5.7)$$

Note that, as expected, the two multipliers k_1 and k_2 play the same role and all the expressions are symmetrical in the exchange of k_1 and k_2 .

As discussed in the previous section, we expect a contribution to the field theory result from the limit $\eta_1 \rightarrow 1$ (together with $k_1, k_2 \rightarrow 0$); in this case, the appropriate change of variables is

$$t_1 = -\alpha' \log k_1, \quad t_2 = -\alpha' \log k_2, \quad t_3 = -\alpha' \log(1 - \eta_1). \quad (5.8)$$

Introducing the mass m^2 to regulate quadratic poles in the usual way, and neglecting terms suppressed as $\alpha' \rightarrow 0$, Eq. (5.6) in this region yields

$$A_{0,\text{red}}^{(2)} = \frac{N^3}{(4\pi)^d} \frac{g_3^2}{2} \int_0^\infty dt_3 \int_0^\infty dt_2 \int_0^{t_2} dt_1 e^{-m^2(t_1+t_2+t_3)} (t_1 t_2)^{-d/2}. \quad (5.9)$$

Since Eq. (5.9) is symmetrical in t_1 and t_2 , it is possible to perform the integration over t_1 and t_2 independently from 0 to ∞ by introducing a factor of $1/2$. In this way one obtains the same result of the reducible vacuum bubble of the Φ^3 field theory defined by Eq. (3.6), including the correct normalization. Again, the factor of $1/4$ in the normalization of this diagram in field theory is a combination of color and symmetry factors, which are unified in the present approach.

The second expected contribution comes from the limit $\eta_1 \rightarrow 0$ and should give the irreducible vacuum diagram. In this case each loop is made by two different

propagators, and this suggests a different identification between field theory proper times and string variables. In fact, the experience acquired at one loop leads us to expect that the multipliers k_i should be associated with the length of an entire loop. Thus we set

$$q_1 = \frac{k_2}{\eta_1} = e^{-t_1/\alpha'} , \quad q_2 = \frac{k_1}{\eta_1} = e^{-t_2/\alpha'} , \quad q_3 = \eta_1 = e^{-t_3/\alpha'} . \quad (5.10)$$

With this choice, Eq. (5.6) becomes

$$A_{0,\text{irr}}^{(2)} = \frac{N^3}{(4\pi)^d} \frac{g_3^2}{2} \int_0^\infty dt_3 \int_0^{t_3} dt_2 \int_0^{t_2} dt_1 e^{-m^2(t_1+t_2+t_3)} \\ \times (t_1 t_2 + t_1 t_3 + t_2 t_3)^{-d/2} . \quad (5.11)$$

Since Eq. (5.11) is completely symmetrical, we can introduce a factor of $1/3!$ and perform the three integrals independently from 0 to ∞ . In this way one correctly reproduces the irreducible vacuum bubble of our Φ^3 theory. Note that by using a single starting formula, Eq. (5.6), we have been able to obtain two diagrams which have a different weight. While in field theory this relative factor of 3 between the two vacuum bubble amplitudes is due to the combination of different combinatorial and color factors, in the string approach this relative normalization appears because Eq. (5.6) has different symmetry properties in the two regions of moduli space that yield the two vacuum bubbles.

It is interesting to see what happens if one considers also non-planar string world-sheets. From Fig. 6, one can see that a non-planar surface may arise if the circle K_1 is centered on the negative axis. The identifications established in the planar case still hold and by following them it is easy to realize that the surface has only one border. When η approaches to zero, the calculations follows exactly the same pattern we have just seen and the result is again the one of Eq. (5.11), but with a factor of N only, instead of N^3 , since here we have only one border. However, if now one tries to mimic the limit which gave the reducible bubble, that is $|\eta| \rightarrow 1$, one sees that there is no singularity in Eq. (5.6). In fact, now η approaches -1 and so it is not possible to associate a Schwinger proper time to the combination $(1-\eta)$: this corner gives a vanishing contribution showing that only the irreducible bubble receive sub-leading corrections in N . By using the equations given in Appendix, it is easy to recover the same result from a field theory analysis.

We conclude our discussion of two-loop vacuum bubbles by briefly considering the single diagram arising in the case of quartic interaction. Here we see at work the mechanism that was suggested for the one-loop Φ^4 tadpole, in Section 4. In fact, the field theory color factor of the vacuum bubble is of the form

$$\mathcal{C} = d_{\alpha\mu}^\alpha d^{\mu\gamma}_\gamma + 2 d_{\alpha\gamma\mu} d^{\alpha\gamma\mu} \\ = 2 N^3 + 2 N (N^2 + 1) , \quad (5.12)$$

where we emphasized the different origin of the various factors of N . The symmetry factor, on the other hand, is $1/8$. Using string theory, and the matching condition

Eq. (3.18), one sees that the overall normalization of this diagram in the planar case is $N^3 g_4$. Now, however, one must introduce proper times only for the two multipliers, since there are only two propagators in the diagram. Thus the overall symmetry factor for the completion of the integration region is $1/2$ instead of $1/6$, for both color flow patterns. If we propose to add them, it would appear that the string gives a result too big by factor of two. The solution to this puzzle lies in the observation that in both configurations one needs to integrate over a finite range in η , extending to $\eta \rightarrow 1$, as in Eq. (5.6). One must regulate the singularity as $\eta \rightarrow 1$, without having a proper time associated with $1 - \eta$. Singularities of this kind were studied in Refs. ([15, 22]), and the correct prescription (a ζ function regularization) turns out to be that these integrals yield precisely a factor of $1/2$. Notice that the non-planar contribution can arise only from the irreducible diagram, which justifies the fact that the coefficient of N in Eq. (5.12) is $1/2$ of the coefficient of N^3 .

5.2 Two-point amplitudes

In this section, scalar amplitudes with two external states are considered; in particular, the irreducible diagrams of Fig. 7 are derived directly from Eq. (2.1), without using the simplified procedure described in [19]. Instead, we follow the procedure just employed for the vacuum bubbles and, for each diagram, we look at the appropriate corners of the integration region of the various string variables. The new

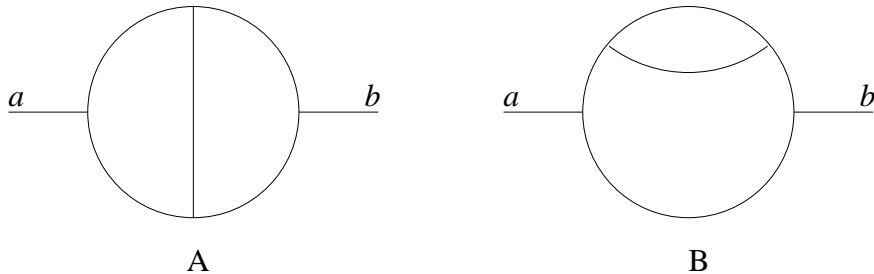


Figure 7: Irreducible two-loop diagrams contributing to the two-point function of the Φ^3 theory.

ingredients needed in Eq. (2.1) in presence of external particles are the two-loop bosonic Green function and, if one wants to extrapolate the result off-shell, the new expressions of the local coordinates $V'_i(0)$. It was shown in [19, 20] that from the Green function in Eq. (2.5) the general structure of two-loop Φ^3 diagrams can be recovered. Moreover Roland and Sato showed in [20] that the string master formula (2.1), reduces to the particle theory amplitudes in the world-line approach, even in the multi-loop case. However, in those papers there is no derivation for the region of integration over the punctures z_i ; this should be given in terms of the parameters determining the shape of two-loop world-sheet. Lacking this information, it is difficult to fix the correct normalizations of the various diagrams, since different

corners of the region of integration over the punctures can contribute to the same field theory diagram. We will now show that, in order to determine the integration region for the punctures z_i , it is sufficient to use the simple geometrical description of Fig. 6, and the analysis of vacuum amplitudes outlined in the previous sections. In fact, as discussed in the Introduction, a general feature of the string approach is that the calculations of diagrams with different number of external legs are closely related to each other. For instance, it is clear from the analysis of vacuum bubbles that, in order to construct irreducible diagrams, the limit $\eta_1 \rightarrow 0$ must be considered. At this point one can freeze the world-sheet shape and put the punctures in all possible configurations on the three borders, remembering that, since we are interested in planar amplitudes, both states must lie on the same boundary of the two-annulus.

Let us start by considering the case in which the punctures are inserted on the internal boundary represented by the segment (AA') . They should then be integrated in the interval $[-1/\sqrt{k_2}, \sqrt{k_2}]$. Analogously, if they are on the other internal boundary, the region of integration is the interval $[D, D']$, while for the contributions of the external boundary each z_i must be allowed to range between B and C , and between C' and B' . In the configuration with small multipliers ($q_i \rightarrow 0$) the world-sheet becomes a graph, and each boundary degenerates into the union of two distinct field theory propagators. It is interesting to note that it is possible to identify the specific corners of moduli space associated with each first quantized field theory diagram, already at the string level. In fact, if $z \in [A', A]$, the contributions obtained correspond to a diagram with the external particles always attached to the first loop; but it turns out that they are emitted from the propagator shared by the two loops if $z \in [-1, -\eta_1]$, while the intervals $z \in [-\eta_1, A]$ and $z \in [A', -1]$ correspond to emission from the propagator not shared with the second loop.

In order to show that this identification is correct, let us calculate the two-loop diagram with one external state in the region $[-1, -\eta_1]$ and the other in the region $[A', -1]$ that should contribute to the first diagram of Fig. 7. As for the local coordinates, here we impose again that $V'_i(0) = |z_i|$, since the punctures are on a border that, from the point of view of the Schottky parametrization, is identical to the one encountered in the one-loop case. Of course, other choices lead to the correct result [19, 21] and only a Yang-Mills calculation, where higher-order terms in q_i are relevant, can discriminate among the various options. In this region, the variable U of Eq. (2.6) can be approximated as $U \sim |z_1|^{-1}$. Thus from Eq. (2.1) one can derive a first contribution to the diagram in Fig. 7, by treating the quadratic poles of the q_i variables in the usual way, and by introducing proper times t_i as in Eq. (5.10). One finds

$$\begin{aligned}
A_a^{(2)}(p_1, p_2) &= \frac{N^2}{(4\pi)^d} \frac{g_3^4}{4} \delta^{ab} \int_0^\infty dt_2 \int_0^{t_2} dt_1 \int_0^{t_1} dt_3 \int_0^{\frac{1}{2}(t_2+t_3)} dt_{z_1} \int_0^{t_3} dt_{z_2} \\
&\times e^{-m^2(t_1+t_2+t_3)} \Delta^{-d/2} \exp [p_1 \cdot p_2 G_a(t_1, t_2, t_3, t_{z_1}, t_{z_2})] \quad , \quad (5.13)
\end{aligned}$$

where the Green function for this diagram is given by

$$G_a(t_1, t_2, t_3, t_{z_1}, t_{z_2}) = t_{z_1} + t_{z_2} - \Delta^{-1} \left((t_1 + t_2)t_{z_2}^2 + (t_1 + t_3)t_{z_1}^2 + 2t_{z_1}t_{z_2}t_1 \right), \quad (5.14)$$

and where $\Delta = (t_1t_2 + t_1t_3 + t_2t_3)$. The Schwinger proper times t_{z_i} are related, as expected, to the positions of the punctures by $t_{z_i} = -\alpha' \log |z_i|$. It can be checked that the integrand of Eq. (5.13) is exactly what one expects from a field theory calculation, but the region of integration over proper times appears strange. In fact, the whole expression is not symmetric in the exchange of any two proper times, as happened in the vacuum diagram of Eq. (5.11). Thus, it is not possible to immediately complete the integration of t_1 and t_3 up to infinity; moreover from the field theory analysis one would expect the proper time t_{z_1} to vary between 0 and t_2 , while the string result covers only part of this region.

These problems are treated by taking into account also the other corners of the integration over the punctures that contribute to the field theory diagram of Fig. 6. For instance, another configuration that should be considered is $z_2 \in [-\eta, -\sqrt{k_2}]$ with z_1 remaining in the same interval as before. In this case U can be approximated as $U \sim \eta/|z_2|$, and from Eq. (2.1) one gets

$$\begin{aligned} A_b^{(2)} &= \frac{N^2}{(4\pi)^d} \frac{g_3^4}{4} \delta^{ab} \int_0^\infty dt_2 \int_0^{t_2} dt_1 \int_0^{t_1} dt_3 \int_{t_3}^{\frac{1}{2}(t_2+t_3)} dt_{z_1} \int_0^{t_3} dt_{z_2} e^{-m^2(t_1+t_2+t_3)} \\ &\times \Delta^{-d/2} \exp [p_1 \cdot p_2 G_b(t_1, t_2, t_3, t_{z_1}, t_{z_2})] \quad , \end{aligned} \quad (5.15)$$

where

$$\begin{aligned} G_b(t_1, t_2, t_3, t_{z_1}, t_{z_2}) &= t_{z_1} - t_{z_2} - \Delta^{-1} \left[(t_2 + t_3)(t_3 - t_{z_2})^2 \right. \\ &\quad \left. + (t_1 + t_3)(t_{z_1} - t_{z_2})^2 - 2(t_{z_2} - t_{z_1})(t_{z_2} - t_3)t_3 \right] . \end{aligned} \quad (5.16)$$

These results seem completely different from Eq. (5.13), and in fact it is difficult to relate them to the diagram of Fig. 6, since the Green function is not the one expected. However, this happens just because Eq. (5.15) is not expressed in terms of the most convenient variables; in fact, by changing $t_{z_1} \rightarrow t_2 + t_3 - t_{z_1}$ the integrand in Eq. (5.15) becomes exactly that of Eq. (5.13) and the region of integration over t_{z_1} becomes the interval $[\frac{1}{2}(t_2 + t_3), t_2]$. At this point the two contributions can be summed by simply extending the integration of t_{z_1} from 0 to t_2 and, as far as the punctures are concerned, the expected field theory result are obtained. Note that the integrand of Eq. (5.13) is symmetric under the simultaneous exchanges $t_{z_1} \leftrightarrow t_{z_2}$, $t_2 \leftrightarrow t_3$, as the world-sheet representation of these regions of integration suggests (see Fig. 8). This consideration suggests that the symmetry in the exchange among t_1 , t_2 and t_3 must be obtained only when the external states are put on the other two boundaries. In fact, when the two punctures are on the boundary (D, D') the final result is exactly that of Eq. (5.13), but with the roles of t_2 and t_1 exchanged. Some changes should however be introduced into the procedure, since this border is not in the usual “one-loop form” (that is with the multipliers at 0 and ∞). First,

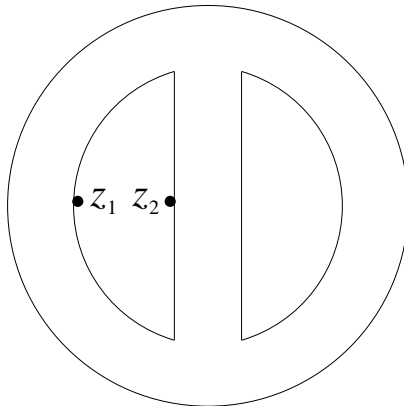


Figure 8: The world-sheet representation of the two-loop contribution derived in the text.

the local coordinates should be expressed in terms of the abelian differential of this loop; second, the variables z_i are not the ones that are directly related to the Schwinger proper times. In fact, the minimum value of z , in this configuration, is D (5.1) and not $\sqrt{k_1}$ as one should expect from the symmetry with the case just considered. In this case the string variable directly related to the Schwinger proper time is

$$x = \left(\frac{z - \eta}{z - 1} \right) , \quad (5.17)$$

which ranges in the interval $[-\frac{1}{\sqrt{k_1}}, -\sqrt{k_1}]$, as expected by symmetry. With these changes, the analysis of the integration on the second boundary is completely similar to the one discussed above.

The contributions coming from the configurations with the punctures on the external boundary can be calculated along the same line. For the local coordinate one can choose the most symmetric combination of the two abelian differentials, since this border surrounds both loops

$$V'_i(0)^{-1} = \omega_1 + \omega_2 . \quad (5.18)$$

The complete result will now be the combination of four regions, corresponding to $z_1 \rightarrow B, B'$ and $z_2 \rightarrow C, C'$. The four regions combine into a single integral, as happened before for the two contributions (5.13) and (5.15), and give the same result as Eq. (5.13) with t_3 and t_1 exchanged.

Taking into account all boundaries, one gets a completely symmetric expression, that should be further multiplied by a factor of two, since in all the computations presented the role of z_1 and z_2 can be exchanged, as was discussed after Eq. (2.2). At this point one can perform the integration over t_1 , t_2 and t_3 independently, introducing, a factor of $1/3!$ that cancels the factor of two coming from the $z_1 \leftrightarrow z_2$ symmetry, and the triple counting arising from the three different first quantized

diagrams. Thus the complete contribution for the field theory configuration of Fig. 6 is simply

$$A_a^{(2)}(p_1, p_2) = \frac{N^2}{(4\pi)^d} \frac{g_3^4}{4} \delta^{ab} \int_0^\infty dt_1 \int_0^\infty dt_2 \int_0^\infty dt_3 \int_0^{t_2} dt_{z_1} \int_0^{t_3} dt_{z_2} e^{-m^2(t_1+t_2+t_3)} \\ \times \Delta^{-d/2} \exp [p_1 \cdot p_2 G_a(t_1, t_2, t_3, t_{z_1}, t_{z_2})] , \quad (5.19)$$

that is, the expected result.

By using the identification among field theory propagators and regions of integration, it is possible to derive also, in a similar way, the other irreducible two-point Φ^3 diagram. This diagram has different symmetries, which implies, in field theory, that its normalization differs from the one of Eq. (5.19) by a factor of two. Without entering into the details of the calculations, it is easy to see the string origin of this difference. In fact, as should be clear from Fig. 9, in this case it is possible to consider two world-sheet configurations for each first quantized diagram, beyond the usual exchange between the external legs z_1 and z_2 ; this fact is eventually responsible for the different normalization. The result is

$$A_c^{(2)}(p_1, p_2) = \frac{N^2}{(4\pi)^d} \frac{g_3^4}{2} \delta^{ab} \int_0^\infty dt_1 \int_0^\infty dt_2 \int_0^\infty dt_3 \int_0^{t_2} dt_{z_1} \int_0^{t_{z_1}} dt_{z_2} e^{-m^2(t_1+t_2+t_3)} \\ \times \Delta^{-d/2} \exp [p_1 \cdot p_2 G_c(t_1, t_2, t_3, t_{z_1}, t_{z_2})] , \quad (5.20)$$

where

$$G_c(t_1, t_2, t_3, t_{z_1}, t_{z_2}) = \Delta^{-1}(t_{z_1} - t_{z_2}) (\Delta - (t_1 + t_3)(t_{z_1} - t_{z_2})) . \quad (5.21)$$

This detailed analysis shows that, in the scalar case, the final form of the whole

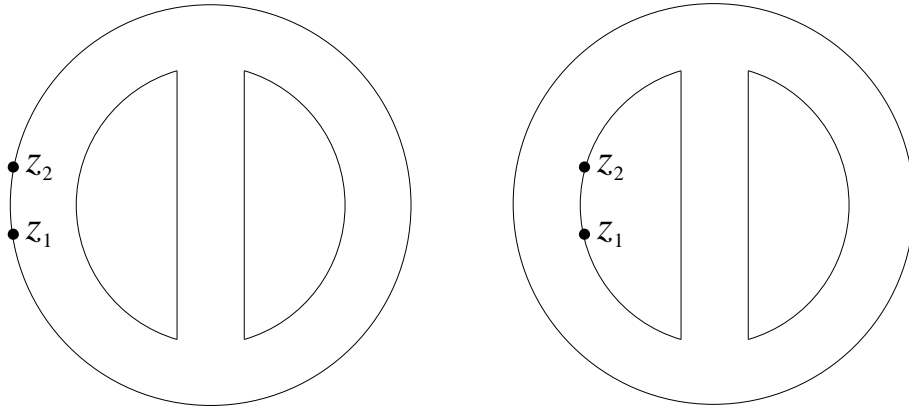


Figure 9: Two different world-sheet configurations that contribute to the same first quantized diagram

calculation can be simply determined by picking one of the various corners of integrations that are relevant for each diagram. All the other contributions only

transform the regions of integration into the expected ones. This step can also be done by hand, by counting the number of configurations contributing to the diagram, and dividing it by the factor of $1/3!$ needed to perform the integration independently. However, if the symmetrization is carried out explicitly, it gives a non-trivial check on the correctness of the result, that can be useful when computing more complicated amplitudes.

We turn very briefly to the case of quartic interactions, by considering the diagram in Fig. 10. The simplest way to get the correct result for this diagram is

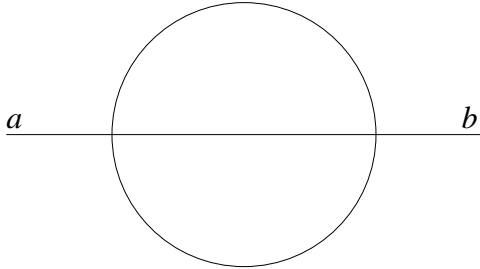


Figure 10: Two-loop two-point diagram in the Φ^4 theory.

perhaps to use the technique that was briefly mentioned in Section 3, when the Φ^4 matching was performed by inserting δ functions for the proper times that must vanish in order to obtain quartic vertices. Choosing for example the boundary $[A, A']$ in Fig. 6, one sees that the punctures must be integrated between $-1/\sqrt{k_1}$ and $-\sqrt{k_1}$. After splitting the integration region into field theory propagators, as was done to obtain the Φ^3 diagrams, we can simply insert the appropriate δ functions, say $\delta((t_{z_1} - t_2)/\alpha')$, with strength $1/2$ since they are all located at the boundaries of the integration regions. Four ways of inserting two such δ functions yield an overall factor of unity. Including the other boundaries in the same way to complete the integration region yields

$$A_2^{(2)} = \frac{g^4}{(4\pi)^d} N^2 \delta^{ab} \int_0^\infty dt_1 \int_0^\infty dt_2 \int_0^\infty dt_3 \Delta^{-d/2} e^{-m^2(t_1+t_2+t_3)+p^2 t_1 t_2 t_3 / \Delta} \quad , \quad (5.22)$$

which is the leading color structure of the field theory diagram we wanted to reproduce.

5.3 Four-point amplitudes

As a last non-trivial check of our technique for Φ^3 amplitudes, we have computed the two-loop four-point diagram depicted in Fig. 11. To extract this diagram from the general expression of the string master formula Eq. (2.1), we can proceed in two steps: first, since we are interested in an irreducible configuration, we have to consider the limit $\eta_1 \rightarrow 0$ and introduce the change of variables Eq. (5.10), which

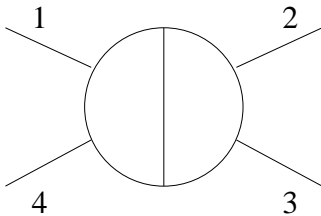


Figure 11: Two-loop four-point diagram in the Φ^3 theory.

generates the structure of the irreducible two-loop vacuum bubble; then we have to consider all possible ways of inserting the four punctures. Two conditions must be respected: the cyclic order is fixed, say to $(1, 2, 3, 4)$, and the pairs of external legs 4, 1 and 2, 3 must attach to different propagators. For example, considering the boundary corresponding to the interval $[A', A]$ in Fig. 6, we can place 1 and 2 inside the interval $[-1, -\eta_1]$ and 2 and 3 outside, or viceversa. Similar reasonings apply to the other two boundaries. Thus, introducing proper times for all the z_i variables and summing up all the contributions, we obtain the expression

$$\begin{aligned}
A_4^{(2)}(p_1, \dots, p_4) &= \frac{N^2}{2} \text{Tr}(\lambda^{a_1} \dots \lambda^{a_4}) \frac{g_3^6}{(4\pi)^d} \int_0^\infty dt_1 \int_0^\infty dt_2 \int_0^\infty dt_3 \\
&\times \int_0^{t_3} dt_{z_1} \int_0^{t_{z_1}} dt_{z_4} \int_0^{t_1} dt_{z_2} \int_0^{t_{z_2}} dt_{z_3} e^{-m^2(t_1+t_2+t_3)} \Delta^{-d/2} \\
&\times \exp[p_1 \cdot p_2 G_a(t_2, t_1, t_3, t_{z_2}, t_{z_1}) + p_1 \cdot p_3 G_a(t_2, t_1, t_3, t_{z_3}, t_{z_1}) \\
&\quad + p_2 \cdot p_4 G_a(t_2, t_1, t_3, t_{z_2}, t_{z_4}) + p_3 \cdot p_4 G_a(t_2, t_1, t_3, t_{z_3}, t_{z_4}) \\
&\quad + p_2 \cdot p_3 G_c(t_2, t_1, t_3, t_{z_2}, t_{z_3}) + p_1 \cdot p_4 G_c(t_2, t_3, t_1, t_{z_1}, t_{z_4})] \{5,23\}
\end{aligned}$$

where the functions G_a and G_c have been defined in Eqs. (5.14) and (5.21) respectively. This result is exactly the leading color term of the field theory diagram of Fig. 11 as expected.

6 Concluding remarks

In this paper we analyzed in detail the method to define and compute field theory limits of string amplitudes and studied in particular the case of scalar states. Conceptually, the target field theory is identified by isolating in the string amplitude the quantities that have to be kept fixed when α' goes to zero. This step is essentially determined by looking at the simplest diagram, as was done in Section 3; in this way one can establish a mapping between g_S and the coupling constant of the field theory one wants to reproduce. After having done this, it is possible to introduce immediately the dimensional Schwinger parameters t_i which measure the length of the various propagators in units of α' . This operation absorbs the

residual dependence on the string tension contained in the overall normalization, so that it becomes possible to take the limit $\alpha' \rightarrow 0$, keeping the field coupling constant and proper times t_i fixed. The mapping between string logarithms and Schwinger parameters is usually rather intuitive. As was stressed through the various calculations, it is quite easy to follow, from a geometrical point of view, how the string world-sheet degenerates into a graph and how to relate each corner of the integration region to a specific Feynman diagram.

In all our calculations, we have always found a precise matching between the string results and the field theory Feynman diagrams. We think that this work shows that string techniques are by now mature, and can be confidently used to simplify the computation of many quantities in field theory. The results obtained in this way can be firmly trusted; in fact, the derivation of the combinatorial factors is easier and the tedious algebra of color decomposition is avoided. Moreover, during the calculation itself, one has the possibility to perform novel consistency checks. For instance, in two-loop calculations one has to obtain the same result from very different regions of the string moduli space. We have shown that this is necessary in order to reconstruct the region of integration over the Schwinger proper times that is expected from field theory.

The generalization of this approach to the physically interesting case of Yang–Mills theory is, of course, computationally more complicated. One has to deal with the derivatives of the Green function, and all stringy quantities have to be expanded up to first order in the multipliers, since the spin-1 particle is not the ground state of the bosonic theory. Furthermore, besides the technical problem, there is also a conceptual difference. As we discussed, the 3 two-loop moduli k_1 , k_2 and η are on the same footing from the field theory point of view; in fact, they are all associated to Φ^3 propagators. Their role in the Schottky parametrization is, however, quite different, since only the k 's are really multipliers, while η is a fixed point. This asymmetry is not evident in the study of Φ^3 diagrams and one obtains directly from the string expression the correct results, with the expected *field theory* symmetry. For instance, Eq. (5.20) is invariant under the exchange of t_1 and t_3 . However, it is already clear from the study of Yang–Mills vacuum bubbles [22], that the different origin of the various parameters in the Schottky description plays a non-trivial role in this more complicated case. We think that the study of the world-sheet geometry will provide other useful information for the derivation of pure glue amplitudes from the string master formula, and we hope that our analysis is a further step in this direction.

Acknowledgements

We would like to thank R. Marotta and F. Pezzella for presenting to us their results about Φ^4 theory before publication, and for many instructive discussions.

We wish also to thank P. Di Vecchia, A. Lerda and S. Sciuto for many useful discussions and suggestions. This work has been partially supported by the EEC under TMR contract ERBFMRX-CT96-0045 and by the Fond National Suisse.

Appendix

We collect in this Appendix the Feynman rules for the scalar theories we are considering, our conventions and several useful formulas concerning computation of color factors.

The Feynman rule for the cubic scalar vertex described by the lagrangian in Eq. (3.6) is simply

$$V_{\alpha\beta\gamma} = i g_3 d_{\alpha\beta\gamma} \quad , \quad (\text{A.1})$$

where $d_{\alpha\beta\gamma}$ is the completely symmetric $U(N)$ color tensor, described below. Similarly, for the quartic interaction in Eq. (3.15), the rule is

$$V_{\alpha\beta\gamma\delta} = i g_4 \left(d_{\alpha\beta\mu} d_{\gamma\delta}^{\mu} + d_{\alpha\gamma\mu} d_{\beta\delta}^{\mu} + d_{\alpha\delta\mu} d_{\beta\gamma}^{\mu} \right) \quad . \quad (\text{A.2})$$

Notice that in field theory we use the standard metric $(+, -, -, -)$, whereas string theory is naturally formulated in the metric with the opposite sign.

To derive the $U(N)$ color algebra, it is useful to start from $SU(N)$ matrices, and then complement them with the diagonal $U(1)$ generator. In the following we will denote $U(N)$ indices with greek letters, $\{\alpha, \beta, \dots\}$, and $SU(N)$ indices with latin ones, $\{a, b, \dots\}$, so that, say, $\alpha = \{0, a\}$ if we assign the value 0 to the $U(1)$ index. Throughout the paper, most of the calculations have been performed with external particles restricted to the $SU(N)$ subgroup, unless explicitly stated. We normalize our generators as

$$\text{Tr}(\lambda_{\alpha}\lambda_{\beta}) = \frac{1}{2}\delta_{\alpha\beta} \quad . \quad (\text{A.3})$$

With this normalization, the $SU(N)$ generators satisfy

$$\begin{aligned} \lambda_a \lambda_b &= \frac{1}{2} \left[\frac{1}{N} \delta_{ab} \mathbf{1} + (d_{abc} + i f_{abc}) \lambda^c \right] \\ (\lambda_a)^i_j (\lambda^a)^k_l &= \frac{1}{2} \left(\delta_l^i \delta_j^k - \frac{1}{N} \delta_j^i \delta_l^k \right) \quad , \end{aligned} \quad (\text{A.4})$$

where f_{abc} are the $SU(N)$ structure constants, while d_{abc} is the completely symmetric $SU(N)$ color tensor, satisfying

$$\begin{aligned} d_{acd} d_b^{cd} &= \frac{N^2 - 4}{N} \delta_{ab} \\ d_{aef} d_{bg}^f d_c^{ge} &= \frac{N^2 - 12}{2N} d_{abc} \quad . \end{aligned} \quad (\text{A.5})$$

To promote the above equations to $U(N)$ we must add a correctly normalized $U(1)$ generator, which can be taken proportional to the identity matrix,

$$\lambda_0 = \frac{1}{\sqrt{2N}} \mathbf{1} \quad . \quad (\text{A.6})$$

The anticommutation relations for the $U(N)$ generators can then be summarized by

$$\{\lambda_\alpha, \lambda_\beta\} = d_{\alpha\beta\gamma} \lambda^\gamma \quad , \quad (\text{A.7})$$

provided one defines

$$\begin{aligned} d_{ab0} &= \sqrt{\frac{2}{N}} \delta_{ab} \\ d_{a00} &= 0 \\ d_{000} &= \sqrt{\frac{2}{N}} \quad . \end{aligned} \quad (\text{A.8})$$

Note that this implies $d_{\alpha\beta 0} = \sqrt{\frac{2}{N}} \delta_{\alpha\beta}$, as well as $d_{0\alpha}^\alpha = 0$, extending to $U(N)$ the corresponding $SU(N)$ property. Using Eq. (A.9), as well as the fact that $f_{ab0} = 0$, one can generalize Eqs. (A.4) and (A.5) to

$$\begin{aligned} \lambda_\alpha \lambda_\beta &= \frac{1}{2} (d_{\alpha\beta\gamma} + i f_{\alpha\beta\gamma}) \lambda^\gamma \\ (\lambda_\alpha)^i_j (\lambda^\alpha)^k_l &= \frac{1}{2} (\delta_l^i \delta_j^k) \quad , \end{aligned} \quad (\text{A.9})$$

and

$$\begin{aligned} d_{a\gamma\delta} d_b^{\gamma\delta} &= N \delta_{ab} \\ d_{a\beta\gamma} d^{\gamma}_{b\delta} d^{\delta\beta}_c &= \frac{N}{2} d_{abc} \quad . \end{aligned} \quad (\text{A.10})$$

It is worth noticing however that Eq. (A.10) does not smoothly generalize to the case in which one or more of the external indices take their values in the $U(1)$ subgroup. For example one finds

$$\begin{aligned} d_{0\gamma\delta} d_0^{\gamma\delta} &= 2N \\ d_{\alpha\beta\gamma} d^{\alpha\beta\gamma} &= N(N^2 + 1) \\ d_{0\alpha\beta} d^\beta_{b\gamma} d^{\gamma\alpha}_c &= N d_{0bc} \\ d_{0\alpha\beta} d^\beta_{0\gamma} d^{\gamma\alpha}_0 &= 2N d_{000} \quad . \end{aligned} \quad (\text{A.11})$$

Finally, a useful formula to connect between standard Feynman rules and color ordered ones is

$$d_{\alpha\beta\gamma} = 2 \text{Tr} (\lambda_\alpha \{\lambda_\beta, \lambda_\gamma\}) \quad . \quad (\text{A.12})$$

The analogous formula for the structure constants f_{abc} serves the same purpose in QCD.

References

- [1] J. Scherk, *Nucl. Phys.* **B 31** (1971) p. 222.
- [2] A. Neveu and J. Scherk, *Nucl. Phys.* **B 36** (1972) p. 55.
- [3] T. Yoneya, *Nuov. Cim. Lett.* **8** (1973) p. 951.
- [4] J. Scherk, J.H. Schwarz, *Nucl. Phys.* **B 81** (1974) p. 118.
- [5] R.R. Metsaev and A.A. Tseytlin, *Nucl. Phys.* **B 298** (1988) p. 109.
- [6] V.S. Kaplunovsky, *Nucl. Phys.* **B 307** (1988) p. 145, [hep-th/9205068](#).
- [7] V.S. Kaplunovsky, *Nucl. Phys.* **B 382** (1992) p. 436, [hep-th/9205070](#).
- [8] Z. Bern and D.A. Kosower, *Phys. Rev. Lett.* **66** (1991) 1669.
- [9] Z. Bern and D.A. Kosower, *Nucl. Phys.* **B 379** (1992) p. 451.
- [10] Z. Bern, *Phys. Lett.* **B 296** (1992) p. 85.
- [11] Z. Bern, L. Dixon and D.A. Kosower, *Phys. Rev. Lett.* **70** (1993) p. 2677, [hep-ph/9302280](#).
- [12] Z. Bern, L. Dixon and D.A. Kosower, *Ann. Rev. Nucl. Part. Sci.* **46** (1996) p. 109 [hep-ph/9602280](#).
- [13] Z. Bern and D.A. Kosower, *Phys. Rev.* **D 38** (1988) 1888.
- [14] P. Di Vecchia, A. Lerda, L. Magnea and R. Marotta, *Phys. Lett.* **351 B** (1995) p. 445, [hep-th/9502156](#).
- [15] P. Di Vecchia, L. Magnea, A. Lerda, R. Russo and R. Marotta, *Nucl. Phys.* **B469** (1996) p. 235, [hep-th/9601143](#).
- [16] Z. Bern, D.C. Dunbar and T. Shimada, *Phys. Lett.* **B 312** (1993) p. 277, [hep-th/9307001](#).
- [17] Z. Bern, L. Dixon, D.C. Dunbar, M. Perelstein and J.S. Rozowsky, *Nucl. Phys.* **B 530** (1998) p. 401, [hep-th/9802162](#).
- [18] K. Roland, *Phys. Lett.* **289 B** (1992) p. 148.
- [19] P. Di Vecchia, L. Magnea, A. Lerda, R. Marotta and R. Russo, *Phys. Lett.* **B388** (1996) p. 65, [hep-th/9607141](#).
- [20] K. Roland and H. Sato, *Nucl. Phys.* **B 480** (1996) p. 99, [hep-th/9604152](#).
- [21] K. Roland and H. Sato, *Nucl. Phys.* **B 515** (1998) p. 488, [hep-th/9709019](#).

- [22] L. Magnea and R. Russo, in it Proceedings of “DIS 97”, Chicago, USA, 1997, eds. J. Repond and D. Krakauer, AIP Conf. Proc. n. 407, p. 913, [hep-ph/9706396](#); also in it Proceedings of “Beyond the Standard Model V”, Balholm, Norway, 1997, eds. G. Eigen, P. Osland and B. Stugu, AIP Conf. Proc. n. 415, p. 347, [hep-ph/9708471](#).
- [23] Z. Bern, J.S. Rozowsky and B. Yan, *Phys. Lett.* **B 401** (1997) p. 273, [hep-ph/9702424](#); also in it Proceedings of “DIS 97”, Chicago, USA, 1997, eds. J. Repond and D. Krakauer, AIP Conf. Proc. n. 407, p. 908, [hep-ph/9706392](#).
- [24] A. Pasquinucci, K. Roland, *Nucl. Phys.* **B 485** (1997) p. 241, [hep-th/9608022](#).
- [25] L. Cappiello, R. Marotta, R. Pettorino and F. Pezzella, *Mod. Phys. Lett.* **A13** (1998) p. 2433, [hep-th/9804032](#); L. Cappiello, R. Marotta, R. Pettorino and F. Pezzella, *Mod. Phys. Lett.* **A13** (1998) p. 2845, [hep-th/9808164](#); A. Liccardo, R. Marotta and F. Pezzella, *Mod. Phys. Lett.* **A14** (1999) p. 799, [hep-th/9903027](#).
- [26] Z. Bern and D.C. Dunbar, *Nucl. Phys.* **B 379** (1992) p. 562.
- [27] M. J. Strassler, *Nucl. Phys.* **B 385** (1992) p. 145, [hep-ph/9205205](#).
- [28] M.G. Schmidt, C. Schubert, *Phys. Lett.* **B 331** (1994) p. 69, [hep-th/9403158](#).
- [29] C. Schubert, *Acta Phys. Polon.* **B 27** (1996) p. 3965, [hep-th/9610108](#).
- [30] H. Sato and M.G. Schmidt, *Nucl. Phys.* **B 524** (1998) p. 742, [hep-th/9802127](#).
- [31] H. Sato and M.G. Schmidt, *Nucl. Phys.* **B 560** (1999) p. 551, [hep-th/9812229](#).
- [32] P. Di Vecchia, M. Frau, A. Lerda and S. Sciuto, *Nucl. Phys.* **B 298** (1988) p.526.
- [33] See, for example, P. Di Vecchia, “*Multiloop amplitudes in string theory*” in Erice, *Theor. Phys.* (1992), p.16, and references therein.
- [34] R. Marotta and F. Pezzella, [hep-th/9912158](#).
- [35] P. Di Vecchia, F. Pezzella, M. Frau, K. Hornfeck, A. Lerda and S. Sciuto, *Nucl. Phys.* **B 322** (1989) p. 317.
- [36] M.B. Green, J.H. Schwarz and E. Witten, “*Superstring Theory*”, Cambridge University Press (1987).
- [37] V. Alessandrini, D. Amati, M. Le Bellac and D. Olive, *Phys. Rep.* **1** (1971) p. 269.
- [38] K. Roland, *Multiloop Amplitudes in Pure Gauge Theories: The superstring Approach* SISSA/ISAS 131-93-EP (1993).